Article

Discovery Medicine 2026; 38(214): 3557–3576
https://doi.org/10.24976/Discov.Med.202638214.271

Targeting the CDX2/YAP1 Axis: A Potential Regulatory Pathway of Ferroptosis in Gastric Cancer

Danqin Zheng[1], Huajuan Ruan[1], Lihui Yu[1], Mingli Guan[1], Junjie Fan[1], Songjie Zhu[2,*]

[1]Department of Pathology, The First People's Hospital of Lin'an District, 311300 Hangzhou, Zhejiang, China
[2]Department of General Medicine, The First People's Hospital of Lin'an District, 311300 Hangzhou, Zhejiang, China
*Correspondence: wuyuezi123@sina.com (Songjie Zhu)
Submitted: 10 April 2026 Revised: 8 September 2026 Accepted: 16 September 2026 Published: 25 November 2026

Background: Gastric cancer (GC) is a common malignancy with high incidence and mortality worldwide. Despite advances in comprehensive therapies, the prognosis of GC patients remains poor. This study aimed to investigate the regulatory mechanisms involving caudal type homeobox 2 (CDX2), yes1 associated transcriptional regulator (YAP1), and ferroptosis in GC.

Methods: Clinical GC and adjacent tissue samples were analyzed by immunohistochemistry (IHC) to detect CDX2 and YAP1 expression. Clinicopathological correlations, survival analysis, and Spearman correlation analysis were performed to evaluate the clinical significance of CDX2 and YAP1. Chromatin immunoprecipitation (ChIP) and dual-luciferase reporter assays were conducted to verify the transcriptional regulation of YAP1 by CDX2. The effects of CDX2 and YAP1 on GC cell proliferation, viability, migration, and ferroptosis were investigated, with rescue experiments performed using Ferrostatin-1 (Fer-1).

Results: CDX2 and YAP1 were highly expressed in GC tissues compared with paired adjacent non-tumor tissues ($p < 0.001$). High CDX2 and YAP1 expression was associated with lower hemoglobin levels and higher CRP and CEA levels, with all intergroup differences reaching statistical significance ($p < 0.05$). ChIP and luciferase assays confirmed that CDX2 directly binds to the YAP1 promoter and activates its transcription. Compared with control cells, CDX2 knockdown inhibited GC cell proliferation, viability and migration ($p < 0.05$). Mechanistically, CDX2 silencing decreased glutathione peroxidase 4 (GPX4) and solute carrier family 7 member 11 (SLC7A11) expression ($p < 0.01$), while increasing ferrous ion (Fe^{2+}) levels and lipid peroxidation ($p < 0.001$). These phenotypic changes were partially rescued by YAP1 overexpression ($p < 0.05$). Similarly, YAP1 knockdown inhibited GC cell proliferation, viability and migration, accompanied by reduced GPX4 and SLC7A11 expression, increased intracellular Fe^{2+} levels, and enhanced lipid peroxidation ($p < 0.05$). These effects were partially reversed by treatment with the ferroptosis inhibitor Ferrostatin-1 ($p < 0.05$).

Conclusion: CDX2 transcriptionally activates YAP1, thereby inhibiting ferroptosis and promoting gastric cancer cell proliferation, viability and migration. These findings highlight the CDX2/YAP1 axis as a potential therapeutic target for ferroptosis modulation in GC and provide new insights into the molecular mechanisms underlying GC progression.

Keywords: GC; YAP1; CDX2; ferroptosis

Introduction

Gastric cancer (GC) is one of the most prevalent malignant tumors worldwide and represents a major public health burden. According to the latest global cancer epidemiological data, GC ranks fifth in incidence and fourth in mortality globally, with particularly high morbidity and mortality rates in East Asia [1,2]. The development of GC is a multifactorial process involving Helicobacter pylori (Hp) infection, genetic susceptibility, dietary factors, chronic inflammation, and environmental exposures [3,4]. Current treatment strategies for GC include surgery, chemotherapy, radiotherapy, targeted therapy, and immunotherapy [5]. However, despite advances in therapeutic approaches, the overall prognosis of GC remains poor, particularly in advanced and metastatic cases, with a five-year survival rate remaining unsatisfactory [6]. Therefore, identifying novel diagnostic biomarkers, therapeutic targets, and prognostic indicators is urgently needed to improve early detection and clinical outcomes in GC.

Yes1 associated transcriptional regulator (YAP1), a key transcriptional co-activator, plays an essential role in the development of various malignancies [7,8]. A previous study has shown that inhibition of the NF2/Hippo signaling axis in epithelial cells activates YAP1, which promotes ferroptosis by upregulating ferroptosis-related regulators [9]. In contrast, in castration-resistant prostate cancer (CRPC), YAP1 suppresses ferroptosis by enhancing the expression of solute carrier family 1 member 5 (SLC1A5) and glutaminase 1 (GLS1), thereby increasing glutathione peroxidase 4 (GPX4) activity [10]. These findings highlight the context-dependent and diverse roles of YAP1 in ferroptosis regulation across different cancer types. However, the specific role and underlying mechanisms of YAP1-mediated ferrop-

Copyright: © 2026 The Author(s). Published by Discovery Medicine. This is an open access article under the CC BY 4.0 license.
Note: *Discovery Medicine* stays neutral with regard to jurisdictional claims in published maps and institutional affiliations.

tosis in GC remain poorly understood. Chromatin immunoprecipitation (ChIP) assays have revealed that caudal type homeobox transcription factor 2 (CDX2) and hepatocyte nuclear factor 4 alpha (HNF4α) can bind to the enhancer region of YAP1 in Caco-2 cells, suggesting their potential involvement in YAP1 transcriptional regulation and function [11]. Given that CDX2 is minimally expressed in normal gastric tissues but aberrantly expressed during gastric tumorigenesis, particularly in intestinal-type GC progression [12], we further focused on CDX2 as a potential upstream regulator of YAP1.

As a gut-specific transcription factor, CDX2 is essential for maintaining epithelial homeostasis and preventing tumor development [13]. It has been reported to suppress epithelial–mesenchymal transition (EMT) in colorectal cancer by reducing β-catenin stability through transcriptional activation of the tumor suppressor PTEN and inhibition of Snail expression [14]. Conversely, CDX2 can promote Reg IV expression in GC cell lines, thereby enhancing cell migration and invasion [15]. A recent study has further shown that tumor-derived exosomes deliver the long non-coding RNA LINC01091 through the microRNA-128-3p/E74 like ETS transcription factor 4 (ELF4)/CDX2 axis, promoting GC growth and metastasis [16]. Based on these findings, this study aimed to systematically investigate CDX2 and YAP1 expression patterns in clinical GC tissues and to elucidate how CDX2 transcriptionally activates YAP1 to regulate ferroptosis and consequently affect GC cell migration, viability and proliferation.

Methods

Clinical Sample Collection

This retrospective observational cohort study included 80 patients who underwent surgical resection at The First People's Hospital of Lin'an District between May 2020 and May 2023. GC tissues and matched adjacent non-tumorous tissues were collected for subsequent analyses. The inclusion criteria were as follows: (1) patients with primary GC confirmed by preoperative imaging and pathological biopsy; (2) patients who underwent surgical resection for GC, including radical or palliative gastrectomy; (3) treatment-naive patients who had not received any preoperative anti-tumor therapies including radiotherapy, chemotherapy, targeted therapy or immunotherapy; (4) patients without concurrent newly diagnosed malignancies; and (5) patients with a history of non-gastric malignancies who had undergone radical surgical resection and showed no recurrence or metastasis during a ≥3-year follow-up period. Patients were excluded if they met any of the following criteria: (1) severe cardiac, hepatic, renal or other vital organ dysfunction; (2) hematological diseases, immune diseases, infectious diseases, mental disorders, or visual and auditory impairments; (3) incomplete clinicopathological data. All patients were diagnosed with GC and underwent surgery according to the recommendations of the Chinese Society of Clinical Oncology [17]. For further analysis, tumor tissues and matched normal gastric samples (collected 5 cm from the tumor margin) were fixed in 10% formalin (60535ES60, Yeasen, China). This study was approved by the Ethics Committee of The First People's Hospital of Lin'an District (Approval No. Lin'an First People's Hospital Lun Yan Shen No. 21 of 2023).

Clinical Data Collection

Clinical data were extracted from medical records, including age, gender, body mass index (BMI), smoking history, alcohol consumption, diabetes, hypertension, coronary heart disease, family history of cancer, history of gastrointestinal diseases, primary tumor location, histological differentiation, clinical stage, lymph node metastasis, Hp infection, and Lauren classification. Laboratory parameters including hemoglobin, C-reactive protein (CRP), platelet-to-lymphocyte ratio (PLR), and carcinoembryonic antigen (CEA), were obtained from routine preoperative blood test results. Surgical information, including resection extent, operative time, and pathological classification, was also recorded.

Follow-Up

All eligible patients underwent standardized postoperative follow-up, with the follow-up period calculated from the date of gastric resection to May 31, 2025. The median follow-up duration was 12 months. The primary endpoints were 1-year-overall survival (OS) and 1-year-disease-free survival (DFS). OS was defined as the time from surgical resection to all-cause death or the last valid follow-up. DFS was defined as the time from surgical resection to the first occurrence of local recurrence, distant metastasis, or all-cause death. Survival and recurrence data were retrospectively collected from medical records, routine outpatient follow-up records, and telephone follow-up interviews. For patients lost to follow-up, survival data were censored at the date of the last valid contact. Patients with incomplete follow-up information were excluded from the final survival analysis to ensure the reliability of the statistical results.

Immunohistochemistry (IHC) Analysis

Matching adjacent normal tissues and paraffin (8002-74-2, Nanjing Reagents, Nanjing, China)-embedded GC tissues were sectioned. Antigen retrieval was performed using citrate buffer (C2488, Sigma-Aldrich, St. Louis, MO, USA). The sections were blocked with 5% bovine serum albumin (BSA, ST025, Beyotime, Shanghai, China) for one hour at room temperature and then incubated (4 °C) overnight with primary antibodies against CDX2 (ab76541, Abcam, Cambridge, UK) or YAP1 (ab52771, Abcam, Cambridge, UK). After washing with phosphate-buffered saline (PBS, C0221A, Beyotime, Shanghai, China), the sections

were incubated with goat anti-rabbit IgG H&L (HRP) (ab6721, Abcam, Cambridge, UK) for 1 hour. Signals were visualized using a 3,3′-diaminobenzidine (DAB) substrate kit (ab64238, Abcam, Cambridge, UK), followed by counterstaining with hematoxylin (H9627, Sigma-Aldrich, St. Louis, MO, USA). Stained tissue sections were examined under a light microscope (400×, Nikon Eclipse 80i, Tokyo, Japan), with brown staining considered indicative of positive protein expression. CDX2 staining was primarily located in the nucleus, whereas YAP1 staining was detected in both the cytoplasm and nucleus.

IHC Scoring

The IHC scores were calculated by multiplying the staining intensity score by the positive tumor cell proportion score. Staining intensity was graded as 0 (no staining), 1 (weak pale yellow), 2 (tan), and 3 (dark brown). The proportion of positive tumor cells was scored as 0 (0– <5%), 1 (5%–25%), 2 (26%–50%), 3 (51%–75%), and 4 (>75%). A total score ≥4 was defined as positive expression, whereas a score < 4 was defined as negative expression [18]. Two experienced pathologists, blinded to the clinical data, independently evaluated and scored all immunohistochemical results. For stratification of CDX2 and YAP1 expression levels, the median mean optical density (MOD) value of the 80 enrolled GC tissue samples was used as the cut-off value. Patients were divided into high-expression (density ≥ median value) and low-expression (density < median value) groups. The proportion of positive tumor cells and MOD values were quantitatively measured using ImageJ software (version 1.54p, National Institutes of Health, Bethesda, MD, USA).

Spearman Correlation Analysis

Spearman correlation analysis was performed to evaluate the correlation between CDX2 and YAP1 expression levels based on MOD values. Since the expression data did not follow a normal distribution, the Spearman correlation coefficient was used for analysis. All statistical tests were two-sided, and a $p < 0.05$ was considered statistically significant.

Binding Site Prediction

Bioinformatics prediction was performed to identify potential binding sites of the transcription factor CDX2 within the YAP1 promoter region. First, the YAP1 promoter sequence (–2000 bp ~ +50 bp) was obtained from the University of California, Santa Cruz (UCSC) Genome Browser (http://genome.ucsc.edu/). Next, the JASPAR database (https://jaspar.genereg.net/) was used to identify potential CDX2-binding motifs by matching the consensus binding sequences. Finally, candidate CDX2-binding loci within the YAP1 promoter region were determined based on the matching results.

Cell Culture

Human GC HGC-27 cells (AW-CH0138, AnWei-sci, Shanghai, China) and the human gastric mucosal epithelial cell line GES-1 (AW-CH0091, AnWei-sci, Shanghai, China) were cultured in Dulbecco's Modified Eagle Medium (DMEM; C0891, Beyotime, Shanghai, China). KATO III cells (CL-0372, Procell, Wuhan, China) and NCI-N87 cells (AW-CH0267, AnWei-sci, Shanghai, China) were maintained in RPMI-1640 medium (GNM31800, Genomcell, Hangzhou, China). All culture media were supplemented with 1% penicillin-streptomycin (CA005-010, GenDEPOT, Katy, TX, USA) and 10% fetal bovine serum (FBS; C0235, Beyotime, Shanghai, China). Cells were maintained in a humidified environment with 5% CO_2 at 37 °C (D165H, Rwdls, Shenzhen, China). All cell lines were authenticated using short tandem repeat (STR) analysis, and continuous mycoplasma monitoring confirmed the absence of contamination in all cultured cells.

Cell Transfection and Grouping

The CDX2 overexpression plasmid (pRP[Exp]-EGFP-CMV>hCDX2[NM_001265.6]), YAP1 overexpression plasmid (pRP[Exp]-EGFP-CMV>hYAP1[NM_001282101.1]), corresponding negative control (NC), and short hairpin RNA (shRNA) targeting CDX2 (shCDX2, pRP[shRNA]-U6>hCDX2[shRNA#1]) and YAP1 (shYAP1, pRP[shRNA]-U6>hYAP1[shRNA#1]), along with the shRNA negative control (shNC), were provided by VectorBuilder (Suzhou, China). The target sequences of the shRNAs are listed in **Supplementary Table 1**. Following the manufacturer's guidelines, transfections were performed using LipofectamineTM 2000 reagent (11668500, Thermo Fisher Scientific, Waltham, MA, USA). Western blotting and quantitative real-time polymerase chain reaction (qRT-PCR) were performed to evaluate transfection efficiency after 48 hours. HGC-27 cells or KATO III cells were divided into the following groups: the first section included Control, shNC+NC, shCDX2+NC, shNC+YAP1, and shCDX2+YAP1 groups; the second section included Control, shNC, shYAP1, and shYAP1+Ferrostatin-1 (Fer-1). Cells in the Control groups were cultured under normal conditions, whereas cells in the other groups were transfected with the corresponding plasmids and/or shRNAs and incubated for 48 hours. The ferroptosis inhibitor Fer-1 (1 μM; HY-100579, MCE, Monmouth Junction, NJ, USA) was added to the shYAP1+Fer-1 group for an additional 12 hours [19].

Cell Viability

GC cells were digested with trypsin (0.25%, P4201, Beyotime, Shanghai, China) to prepare a single-cell suspension. Cells were then seeded into 96-well plates (100 μL per well; FCP962, Beyotime, Shanghai, China) at a density of 6×10^3 cells per well and cultured for 48 h. Subsequently,

Cell Counting Kit-8 (CCK-8) reagent (10 µL; C0038, Beyotime, Shanghai, China) was added to each well, followed by incubation for 2 h. Absorbance was measured at 450 nm using a microplate reader (Microplate Manager v5.2, Bio-Rad Laboratories, Inc., Hercules, CA, USA). Cell viability was calculated and normalized to that of the Control group, which was set as 100%.

qRT-PCR

TRIzol reagent (R0016, Beyotime, Shanghai, China) was used to extract total RNA, and a SmartSpec Plus spectrophotometer (Bio-Rad Laboratories, Hercules, CA, USA) was used to evaluate the purity of the extracted RNA. Complementary DNA (cDNA) was synthesized using the PrimeScriptTM RT Reagent Kit (RR047A, Takara, Wuhan, China). Subsequently, qRT-PCR was performed using the SYBR Green PCR Master Mix (4344463, Thermo Fisher Scientific, Waltham, MA, USA) on an ABI 7500 Real-Time PCR System (7500 SDS Software v2.0, Thermo Fisher Scientific, Waltham, MA, USA). The primer sequences, provided by RiboBio (China), are listed in **Supplementary Table 2**. Relative gene expression levels were calculated using the $2^{-\Delta\Delta Ct}$ method [20].

Western Blot Analysis

A bicinchoninic acid protein assay kit (P0009, Beyotime, Shanghai, China) was used to quantify the total protein extracted using radioimmunoprecipitation assay (RIPA) buffer (P0013, Beyotime, Shanghai, China). The extracted proteins were separated by 10% sodium dodecyl sulfate-polyacrylamide gel electrophoresis (SDS-PAGE; P0012A, Beyotime, Shanghai, China) and subsequently transferred onto polyvinylidene fluoride (PVDF) membranes (FFP24, Beyotime, Shanghai, China). After blocking with 5% bovine serum albumin (BSA; ST023, Beyotime, Shanghai, China) for 1 h, the membranes were incubated overnight (4 °C) with primary antibodies (1:1000; **Supplementary Table 3**). The membranes were then washed and incubated with secondary antibodies (1:50000; **Supplementary Table 3**) for one hour at room temperature. Signals were detected using the ChemiDocTM XRS imaging system (Bio-Rad Laboratories, Inc., Hercules, CA, USA) with BeyoECL Star chemiluminescent substrate (P0018AS, Beyotime, Shanghai, China). Band intensities were quantified using ImageJ (version 1.54p, National Institutes of Health, Bethesda, MD, USA) software. Relative protein expression levels were normalized to the Control group, which was set as 1.

Dual-Luciferase Reporter Assay

A wild-type YAP1 promoter luciferase reporter plasmid (YAP1-WT) was constructed using the pGL3-Basic vector, which was purchased from Promega (E1330, Madison, WI, USA), based on the predicted CDX2 binding sites within the YAP1 promoter region identified using the JASPAR database. As a negative control, a mutant YAP1 promoter (YAP1-MUT) with disrupted CDX2 binding sites was generated. In all experimental groups, the corresponding CDX2 overexpression or empty vector plasmid, YAP1-WT/YAP1-MUT reporter plasmid, and pRL Renilla Luciferase Reporter Vectors (E2231, Promega, Madison, WI, USA) were co-transfected into HGC-27 cells. Following the manufacturer's instructions, luciferase activity was measured 48 hours after transfection using the Dual-Luciferase® Reporter Assay System (E1910, Promega, Madison, WI, USA). Relative luciferase activity was calculated by normalizing Firefly luciferase activity to the corresponding Renilla luciferase signal.

ChIP Assay

A ChIP assay kit (P2078, Beyotime, Shanghai, China) was used to perform the ChIP assay. First, HGC-27 cells were cross-linked with 1% formaldehyde (252549, Sigma, St. Louis, MO, USA) for 10 minutes. The reaction was then quenched with Glycine solution (ST085, Beyotime, Shanghai, China). After washing and detachment from the plates, cells were resuspended in buffer containing 1 mM phenylmethylsulfonyl fluoride (PMSF; ST505, BioTech, Shanghai, China). Following centrifugation and collection, the cells were lysed in SDS lysis buffer supplemented with 1 mM PMSF (SL1031, Coolaber, Beijing, China). The lysates were sonicated to fragment chromatin into 200–1000 bp fragments and then centrifuged. After collection of the supernatant, samples were diluted with ChIP dilution buffer and incubated with protein A+G agarose beads pre-blocked with salmon sperm DNA. Immunoprecipitation was performed using an anti-CDX2 antibody (#3977, Cell Signaling Technology, Danvers, MA, USA). Normal IgG (#2729, Cell Signaling Technology, Danvers, MA, USA) was used as the negative control. After washing, the immunocomplexes were incubated with 5 M sodium chloride (S9888, Sigma, St. Louis, MO, USA) and RNase A (10 mg/mL; ST576, Beyotime, Shanghai, China) at 65 °C for four hours. The samples were then treated with proteinase K (20 mg/mL; ST533, Beyotime, Shanghai, China) at 60 °C for 1 h. DNA was purified using a PCR purification kit (28106×4, QIAGEN, Hilden, North Rhine-Westphalia, Germany). Purified DNA samples were subjected to CHIP-qPCR amplification to detect the enrichment of YAP1 promoter fragments bound by CDX2. The enrichment level of target DNA fragments was quantified as fold enrichment relative to the IgG negative control group based on the qPCR results.

All analyses were performed using the human reference genome GRCh38 (hg38). ChIP-qPCR primers were specifically designed to target the proximal promoter region of YAP1, covering the genomic coordinates chr11: 102109624-102109781. The amplified fragment was 158 bp in length and contained a predicted CDX2 binding site. Detailed primer sequences, genomic locations, and amplicon information are provided in **Supplementary Table 4**.

Colony Formation Assay

HGC-27 cells (1000 cells/well) were seeded into 6-well plates (FCP060, Beyotime, Shanghai, China) and cultured for 10 days. Following medium removal, cells were washed with phosphate-buffered saline (PBS; C0221A, Bioinno, Suzhou, China) and fixed with 4% paraformaldehyde (P0099, Beyotime, Shanghai, China) for 15 minutes. Subsequently, colonies were stained using a crystal violet staining kit (C0121, Beyotime, Shanghai, China). After imaging with a digital camera (Nikon, Tokyo, Japan), the number of colonies was counted. All data were normalized to the Control group, which was assigned a colony formation rate of 100%.

Cell Migration Assay

To measure cell migration, Transwell inserts (FTW064, Beyotime, Shanghai, China) were used. The lower chambers were filled with 500 µL of DMEM containing 10% FBS as a chemoattractant, while the upper chambers were seeded with 200 µL of serum-free DMEM containing 5×10^4 of HGC-27 or KATO III cells suspensions. After 24 h, non-migrated cells on the upper surface of the membrane were removed. The migrated cells on the lower surface were fixed with 4% paraformaldehyde (E-IR-R114, Elabscience, Wuhan, China) for 15 minutes and then stained with 0.1% crystal violet for 15 minutes. An inverted microscope (×200, Olympus, Center Valley, PA, USA) was employed to image and count cells in five randomly selected fields for each insert. The number of migrated cells in five random fields per sample was quantitatively determined using ImageJ software (version 1.54p, National Institutes of Health, Bethesda, MD, USA). All results were normalized to the Control group (defined as 100% for the control group).

Lipid Peroxidation Level Measurement

Intracellular lipid peroxidation levels were detected using the C11-BODIPY 581/591 fluorescent probe (HY-DY1022, MCE, Monmouth Junction, NJ, USA) in HGC-27 and KATO III cells after treatment. The harvested cells were resuspended in PBS and incubated with C11-BODIPY 581/591 probe at a final working concentration of 2 µM for 30 minutes. After staining, cells were washed three times with PBS to remove residual unbound probe. Finally, cells were resuspended in PBS and filtered to obtain a single-cell suspension. Flow cytometry (Version 5.1, Becton-Dickinson Biosciences, Franklin Lakes, NJ, USA) using the FITC channel was performed to detect cellular fluorescence intensity. The relative lipid peroxidation levels in each group were normalized to the Control group.

Intracellular Ferrous Ion (Fe^{2+}) Detection

Intracellular Fe^{2+} levels were detected using a commercial iron assay kit (S1068S, Beyotime, Shanghai, China) according to the manufacturer's instructions. HGC-27 and KATO III cells were harvested after treatment and rinsed twice with pre-cooled PBS. Cells were thoroughly lysed, and the supernatant was collected after high-speed centrifugation (4 °C, 12,000 ×g). The supernatant was then incubated with the working solution at room temperature in the dark for 30 minutes. Absorbance was measured at 593 nm using a microplate reader (Microplate Manager v5.2, Bio-Rad Laboratories, Inc., Hercules, CA, USA). The intracellular Fe^{2+} concentration was calculated based on the standard curve, and the relative Fe^{2+} content of each group was normalized to the Control group.

Statistical Analysis

Statistical analyses and plotting were performed using SPSS 20.0 (Version 20.0, IBM Corporation, Armonk, NY, USA) and GraphPad Prism 8 (Version 8.0, GraphPad Software, LLC, Boston, MA, USA). The normality of continuous variables was assessed using the Kolmogorov-Smirnov test. Normally distributed data were expressed as mean ± standard deviation (SD), whereas non-normally distributed data were presented as median [M (P_{25}, P_{75})] and analyzed using the Mann-Whitney U test. Categorical data were expressed as frequencies (percentages) and compared using the Pearson χ^2 test (when all expected cell counts ≥5), Yates' continuity-corrected χ^2 test (when $1 \leq$ expected count < 5 and $N \geq 40$), or Fisher's exact test (when expected count <1 or actual frequency = 0), as appropriate. Ordinal categorical data were analyzed using the Mantel-Haenszel linear-by-linear association χ^2 test. For paired 2 × 2 binary contingency tables (Table 2 and Table 3), the SPSS McNemar procedure provides exact binomial *p*-values but does not report the test statistic for the continuity-corrected McNemar test. Therefore, the continuity-corrected McNemar statistic was manually calculated using the formula ($\chi^2 = (|b - c| - 1)^2 / (b + c)$). The critical values of the χ^2-distribution with df = 1 were used for significance determination: $\chi^2 > 3.841$ for $p < 0.05$; $\chi^2 > 10.828$ for $p < 0.001$. Exact binomial McNemar *p*-values generated by SPSS were additionally used for cross-validation. Paired IHC intensity density scores were analyzed using the paired *t*-test or Wilcoxon signed-rank test according to the normality of paired differences. Survival outcomes were evaluated using Kaplan–Meier survival curves and compared using the Log-rank (Mantel–Cox) test. A *p*-value < 0.05 was considered statistically significant for all analyses.

For cellular experiments, data were obtained from at least three independent replicates and expressed as mean ± SD. Comparisons between two groups were performed using the independent-sample *t*-test, while comparisons among multiple groups were conducted using one-way analysis of variance (ANOVA) followed by Tukey's post-hoc test. A *p*-value < 0.05 was considered statistically significant.

Table 1. Baseline demographic, clinical, pathological, laboratory and surgical characteristics of enrolled GC patients.

Variable		GC patients (N = 80)
Age [n (%)]	≤44	0 (0.00)
	45–59	15 (18.75)
	≥60	65 (81.25)
Gender [n (%)]	Male	51 (63.75)
	Female	29 (36.25)
BMI (kg/m^2)		22.25 ± 2.31
Smoking history [n (%)]		30 (37.50)
Alcohol consumption [n (%)]		36 (45.00)
Diabetes [n (%)]		38 (47.50)
Hypertension [n (%)]		43 (53.75)
Coronary heart disease [n (%)]		47 (58.75)
Family history of cancer [n (%)]		8 (10.00)
History of gastrointestinal diseases [n (%)]	Gastric ulcer	4 (5.00)
	Gastritis	15 (18.75)
	Gastroenteritis	4 (5.00)
	Colon cancer	2 (2.50)
	None	45 (56.25)
	Others	10 (12.50)
Primary tumor location [n (%)]	Upper stomach	30 (37.50)
	Middle stomach	16 (20.00)
	Lower stomach	21 (26.25)
	Overlapping sites	3 (3.75)
	Unspecified	10 (12.50)
Primary tumor diameter [n (%)]	≤2 cm	24 (30.00)
	>2 cm	56 (70.00)
Histological differentiation [n (%)]	Well-differentiated	8 (10.00)
	Moderately differentiated	31 (38.75)
	Poorly differentiated	41 (51.25)
	Undifferentiated	0 (0.00)
Clinical stage [n (%)]	1	30 (37.50)
	2	17 (21.25)
	3	27 (33.75)
	4	6 (7.50)
Lymph node metastasis [n (%)]		42 (52.50)
Hp infection [n (%)]		58 (72.50)
Lauren classification [n (%)]	Intestinal type	15 (18.75)
	Diffuse type	33 (41.25)
	Mixed type	31 (38.75)
	Unclassified	1 (1.25)
Hemoglobin (g/L)		78.46 ± 7.15
CRP (mg/L)		12.53 ± 1.19
PLR		342.15 ± 52.46
CEA (μg/L)		6.37 ± 0.98
Surgical resection extent [n (%)]	Total gastrectomy	25 (31.25)
	Partial gastrectomy	55 (68.75)
Operation time (h)		4.31 ± 0.98
Pathological type [n (%)]	Adenocarcinoma	67 (83.75)
	Signet-ring cell carcinoma	9 (11.25)
	Small cell neuroendocrine carcinoma	1 (1.25)
	Poorly cohesive carcinoma	2 (2.50)
	Tubular adenocarcinoma	1 (1.25)

Abbreviation: BMI, body mass index; CRP, C-reactive protein; PLR, platelet-to-lymphocyte ratio; CEA, carcinoembryonic antigen; Hp, *Helicobacter pylori*.

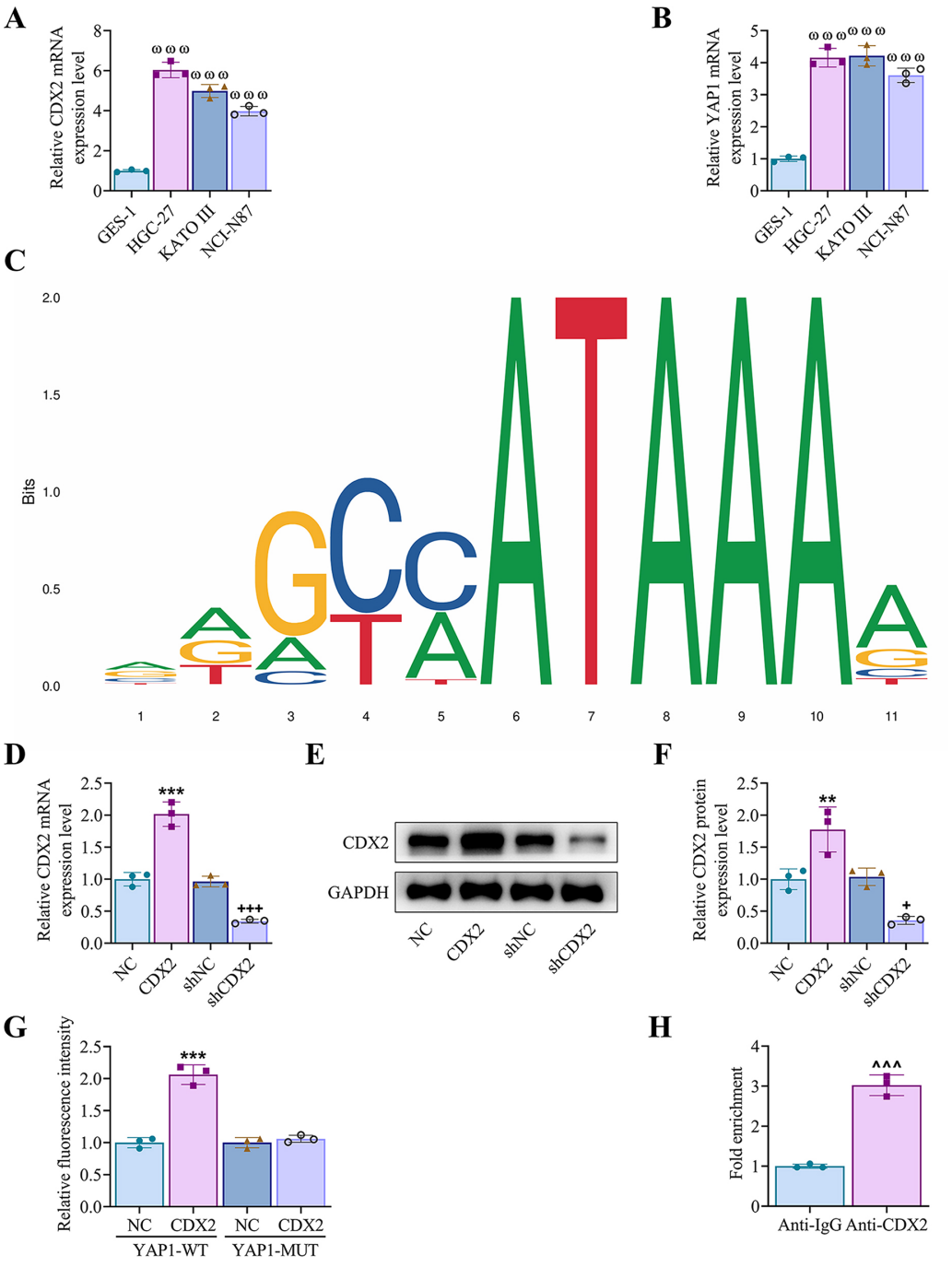

Fig. 1. Caudal type homeobox 2 (CDX2) transcriptionally regulates yes1 associated transcriptional regulator (YAP1). (A,B) Quantitative real-time polymerase chain reaction (qRT-PCR) analysis of CDX2 and yes1 associated transcriptional regulator (YAP1) in GES-1, HGC-27, KATO III and NCI-N87 cells. Glyceraldehyde-3-phosphate dehydrogenase (GAPDH) was used as an internal control. (C) Predicted CDX2 binding motif in the YAP1 promoter region based on the JASPAR database. (D) QRT-PCR analysis of CDX2 expression following transfection with CDX2 overexpression or short hairpin RNA targeting CDX2 (shCDX2) in HGC-27 cells. GAPDH was used as an internal control. (E,F) Western blot analysis of CDX2 expression in HGC-27 cells after transfection with CDX2 overexpression or shCDX2. GAPDH was used as an internal control. (G) Dual-luciferase reporter assay showing the effect of CDX2 on YAP1 promoter activity. (H) Chromatin immunoprecipitation (ChIP) assay confirming CDX2 binding to the YAP1 promoter region. All experiments were independently repeated three times with three biological replicates. $^{\omega\omega\omega}p < 0.001$ vs. GES-1; $^{**}p < 0.01$, $^{***}p < 0.001$ vs. negative control (NC); $^{+}p < 0.05$, $^{+++}p < 0.001$ vs. short hairpin RNA negative control (shNC); $^{\wedge\wedge\wedge}p < 0.001$ vs. Anti-IgG (one-way ANOVA followed by Tukey's multiple comparisons test for panels A, B, D and F; independent-sample *t*-test for panel G and H).

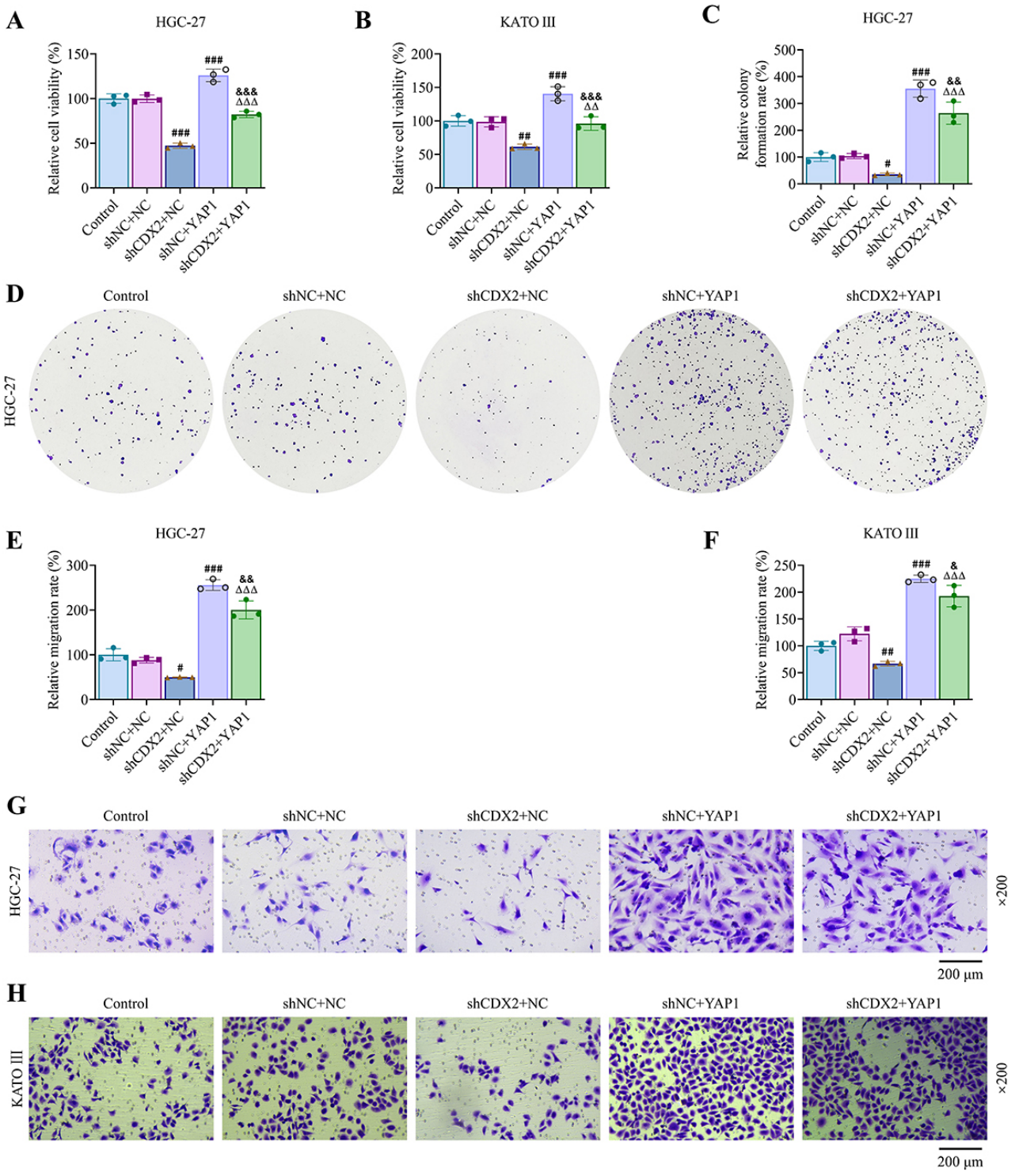

Fig. 2. CDX2 and YAP1 regulate gastric cancer (GC) cell function. (A,B) Cell Counting Kit-8 (CCK-8) assays assessing the viability of HGC-27 and KATO III cells in the following groups: Control, shNC+NC, shCDX2+NC, shNC+YAP1, and shCDX2+YAP1. (C,D) Colony formation assays assessing the proliferative capacity of HGC-27 cells. (E–H) Transwell migration assays evaluating HGC-27 and KATO III cell migration. Magnification: 200×; scale bar: 200 μm. All experiments were independently repeated three times with three biological replicates. $^{\#}p < 0.05$, $^{\#\#}p < 0.01$, $^{\#\#\#}p < 0.001$ vs. shNC+NC; $^{\&}p < 0.05$, $^{\&\&}p < 0.01$, $^{\&\&\&}p < 0.001$ vs. shNC+YAP1; $^{\Delta\Delta}p < 0.01$, $^{\Delta\Delta\Delta}p < 0.001$ vs. shCDX2+NC (one-way ANOVA followed by Tukey's multiple comparisons test).

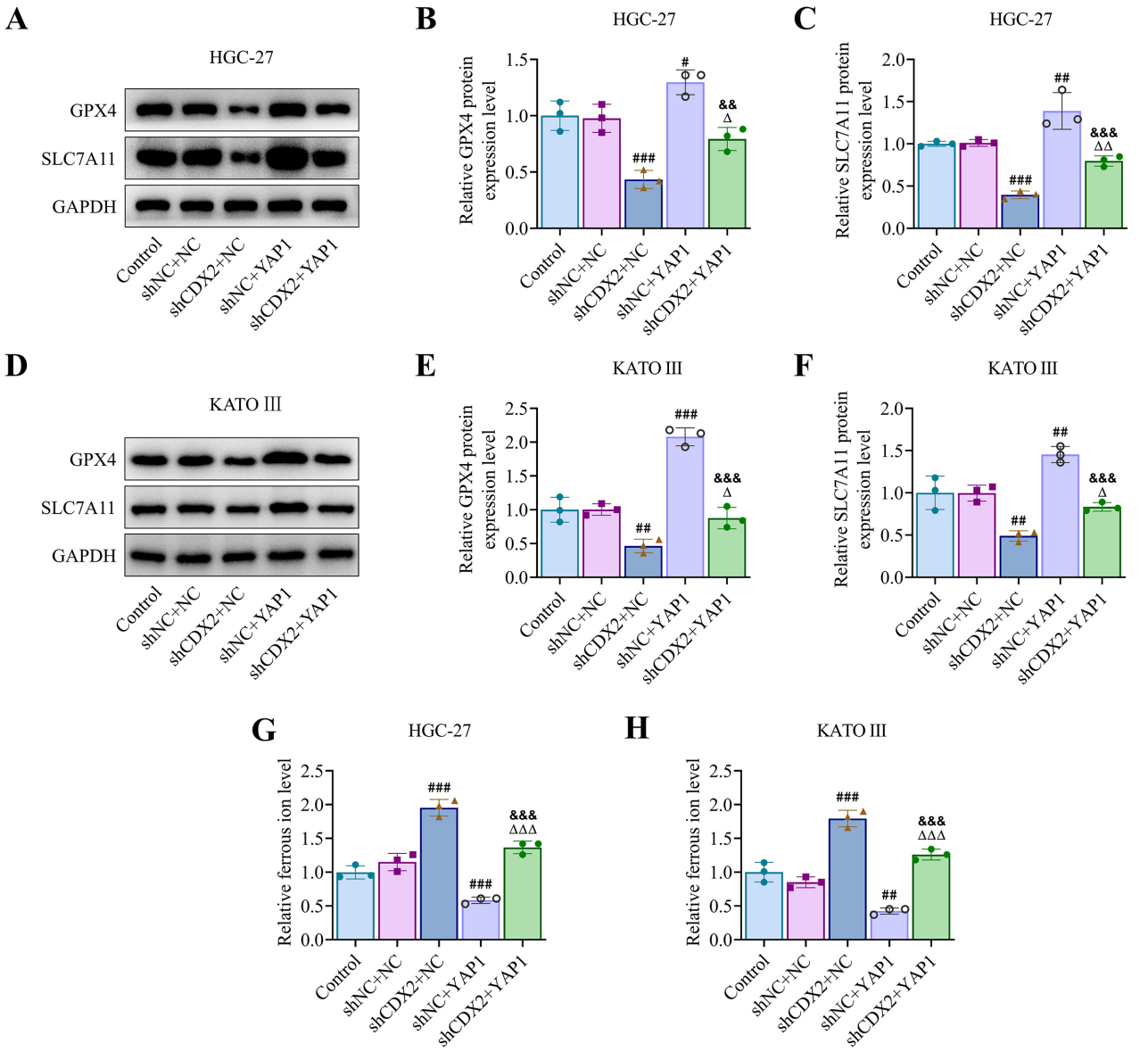

Fig. 3. CDX2 and YAP1 regulate ferroptosis in gastric cancer (GC) cells. (A–F) Western blot analysis of glutathione peroxidase 4 (GPX4) and solute carrier family 7 member 11 (SLC7A11) protein levels in HGC-27 and KATO III cells across different groups. GAPDH was used as an internal control. (G,H) Detection of ferrous ion (Fe^{2+}) levels in HGC-27 and KATO III cells using a commercial kit across the indicated groups, with all data normalized to the Control group. All experiments were independently repeated three times with three biological replicates. $^{\#}p < 0.05$, $^{\#\#}p < 0.01$, $^{\#\#\#}p < 0.001$ vs. shNC+NC; $^{\&\&}p < 0.01$, $^{\&\&\&}p < 0.001$ vs. shNC+YAP1; $^{\Delta}p < 0.05$, $^{\Delta\Delta}p < 0.01$, $^{\Delta\Delta\Delta}p < 0.001$ vs. shCDX2+NC (one-way ANOVA followed by Tukey's multiple comparisons test).

Table 2. Positive expression of CDX2 in gastric cancer and adjacent tissues [n (%)].

	Adjacent normal tissues (+)	Adjacent normal tissues (–)
Gastric cancer tissues (+)	27 (33.75)	51 (63.75)
Gastric cancer tissues (–)	0 (0.00)	2 (2.50)
χ^2		49.020
p		<0.001

Note: (+) indicates positive expression of CDX2, and (–) indicates negative expression of CDX2.

Abbreviations: CDX2, caudal type homeobox transcription factor 2.

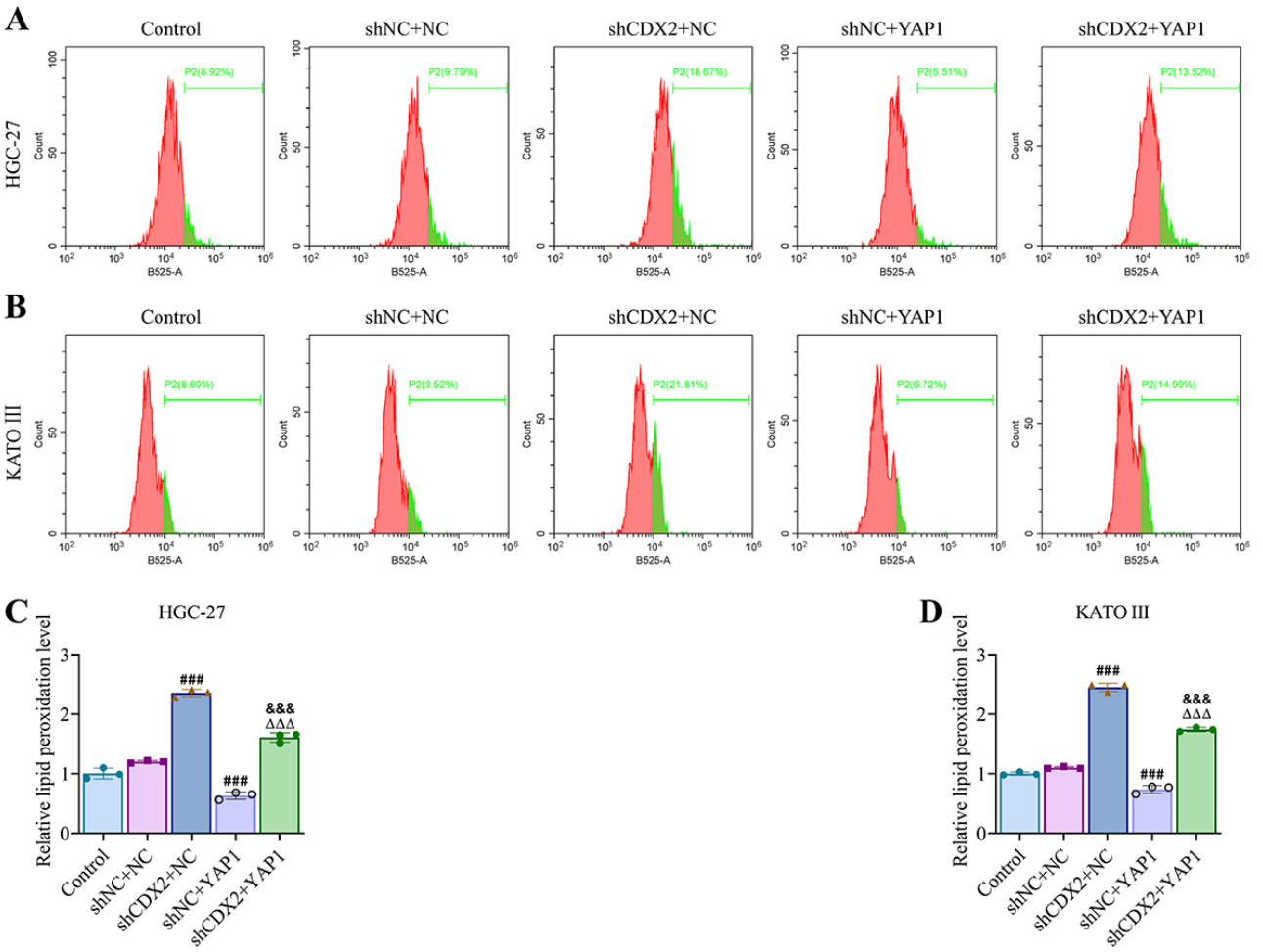

Fig. 4. CDX2 and YAP1 regulate lipid peroxidation in GC cells. (A–D) Detection of lipid peroxidation levels in HGC-27 and KATO III cells using C11-BODIPY 581/591 fluorescent probe, with all data normalized to the Control group. All experiments were independently repeated three times with three biological replicates. $^{###}p < 0.001$ vs. shNC+NC; $^{\&\&\&}p < 0.001$ vs. shNC+YAP1; $^{\Delta\Delta\Delta}p < 0.001$ vs. shCDX2+NC (one-way ANOVA followed by Tukey's multiple comparisons test).

Table 3. Positive expression of YAP1 in gastric cancer and adjacent tissues [n (%)].

	Adjacent normal tissues (+)	Adjacent normal tissues (–)
Gastric cancer tissues (+)	40 (50.00)	40 (50.00)
Gastric cancer tissues (–)	0 (0.00)	0 (0.00)
χ^2		38.025
p		<0.001

Note: (+) indicates positive expression of YAP1, and (–) indicates negative expression of YAP1.

Abbreviations: YAP1, yes1 associated transcriptional regulator.

Results

Clinical Characteristics and Prognostic Outcomes in GC Patients

Among the 80 GC patients, 81.25% were aged ≥60 years (Table 1). The gender distribution showed that 63.75% were male and 36.25% were female. The mean BMI was 22.25 ± 2.31 kg/m^2. Additionally, 10.00% of patients had a family history of cancer. The primary tumor was most frequently located in the upper stomach (37.50%), followed by the lower stomach (26.25%) and middle stomach (20.00%). Histological analysis revealed that most tumors were poorly differentiated (51.25%), while 38.75% were moderately differentiated and 10.00% were well-differentiated. According to clinical staging, 37.50% of patients were classified as stage I, 21.25% as stage II, 33.75% as stage III, and 7.50% as stage IV. Lymph node metastasis was observed in 52.50% of patients, and Hp infec-

Table 4. Correlation between CDX2 high/low expression and clinical pathological characteristics.

Variable		CDX2 low-expression (N = 40)	CDX2 high-expression (N = 40)	$Z/\chi^2/t$	p
Age [n (%)]	≤44	0 (0.00)	0 (0.00)	0.738	0.390
	45–59	9 (22.50)	6 (15.00)		
	≥60	31 (77.50)	34 (85.00)		
Gender [n (%)]	Male	25 (62.50)	26 (65.00)	0.054	0.816
	Female	15 (37.50)	14 (35.00)		
BMI (kg/m^2)		22.57 ± 2.38	21.94 ± 2.23	1.224	0.225
Smoking history [n (%)]		13 (32.50)	17 (42.50)	0.853	0.356
Alcohol consumption [n (%)]		19 (47.50)	17 (42.50)	0.202	0.653
Diabetes [n (%)]		21 (52.50)	17 (42.50)	0.802	0.370
Hypertension [n (%)]		22 (55.00)	21 (52.50)	0.050	0.823
Coronary heart disease [n (%)]		25 (62.50)	22 (55.00)	0.464	0.496
Family history of cancer [n (%)]		2 (5.00)	6 (15.00)	1.250	0.264
History of gastrointestinal diseases [n (%)]	Gastric ulcer	1 (2.50)	3 (7.50)		0.692
	Gastritis	6 (15.00)	9 (22.50)		
	Gastroenteritis	2 (5.00)	2 (5.00)		
	Colon cancer	1 (2.50)	1 (2.50)		
	None	26 (65.00)	19 (47.50)		
	Others	4 (10.00)	6 (15.00)		
Primary tumor location [n (%)]	Upper stomach	19 (47.50)	11 (27.50)	5.531	0.237
	Middle stomach	9 (22.50)	7 (17.50)		
	Lower stomach	7 (17.50)	14 (35.00)		
	Overlapping sites	1 (2.50)	2 (5.00)		
	Unspecified	4 (10.00)	6 (15.00)		
Primary tumor diameter [n (%)]	≤2 cm	14 (35.00)	10 (25.00)	0.952	0.329
	>2 cm	26 (65.00)	30 (75.00)		
Histological differentiation [n (%)]	Well-differentiated	3 (7.50)	5 (12.50)		0.810
	Moderately differentiated	16 (40.00)	15 (37.50)		
	Poorly differentiated	21 (52.50)	20 (50.00)		
	Undifferentiated	0 (0.00)	0 (0.00)		
Clinical stage [n (%)]	1	16 (40.00)	14 (35.00)	0.294	0.769
	2	7 (17.50)	10 (25.00)		
	3	15 (37.50)	12 (30.00)		
	4	2 (5.00)	4 (10.00)		
Lymph node metastasis [n (%)]		23 (57.50)	19 (47.50)	0.802	0.370
Hp infection [n (%)]		28 (70.00)	30 (75.00)	0.251	0.617
Lauren classification [n (%)]	Intestinal type	7 (17.50)	8 (20.00)		1.000
	Diffuse type	16 (40.00)	17 (42.50)		
	Mixed type	16 (40.00)	15 (37.50)		
	Unclassified	1 (2.50)	0 (0.00)		
Hemoglobin (g/L)		81.61 ± 6.39	75.31 ± 6.51	4.372	0.000
CRP (mg/L)		11.99 (11.51, 12.54)	13.12 (12.31, 13.61)	3.556	0.000
PLR		343.45 ± 55.79	340.86 ± 49.58	0.219	0.827
CEA (μg/L)		5.86 (5.53, 6.24)	6.72 (6.38, 7.08)	3.580	0.000
Surgical resection extent [n (%)]	Total gastrectomy	13 (32.50)	12 (30.00)	0.058	0.809
	Partial gastrectomy	27 (67.50)	28 (70.00)		
Operation time (h)		4.44 ± 1.03	4.19 ± 0.93	1.139	0.258

Table 4. Continued.

Variable		CDX2 low-expression (N = 40)	CDX2 high-expression (N = 40)	$Z/\chi^2/t$	p
Pathological type [n (%)]	Adenocarcinoma	34 (85.00)	33 (82.50)		0.737
	Signet-ring cell carcinoma	3 (7.50)	6 (15.00)		
	Small cell neuroendocrine carcinoma	1 (2.50)	0 (0.00)		
	Poorly cohesive carcinoma	1 (2.50)	1 (2.50)		
	Tubular adenocarcinoma	1 (2.50)	0 (0.00)		

Abbreviation: BMI, body mass index; CRP, C-reactive protein; PLR, platelet-to-lymphocyte ratio; CEA, carcinoembryonic antigen; Hp, *Helicobacter pylori*; CDX2, caudal type homeobox transcription factor 2.

tion was positive in 72.50% of cases. Based on the Lauren classification, the diffuse type accounted for the largest proportion (41.25%). The baseline laboratory parameters of the enrolled GC patients are summarized in Table 1: Hemoglobin, 78.46 ± 7.15 g/L; CRP, 12.53 ± 1.19 mg/L; PLR, 342.15 ± 52.46; and CEA, 6.37 ± 0.98 µg/L. The primary outcome indicators were 1-year overall survival (OS) and 1-year disease-free survival (DFS). Among the 80 GC patients, the 1-year OS rate was 82.50% (66 out of 80 patients). After excluding 6 stage IV patients, 22 of the remaining 74 patients experienced disease recurrence, resulting in a 1-year DFS rate of 70.27% (52 out of 74 patients).

Clinicopathological and Prognostic Relevance of CDX2 and YAP1 Expression in Gastric Cancer

IHC results demonstrated that 78 out of 80 GC tissue samples exhibited positive CDX2 expression, corresponding to a positive rate of 97.50%, while all 80 GC tissues showed positive YAP1 staining, with a positive rate of 100.00%. In paired adjacent normal tissues, the positive rates were 33.75% for CDX2 and 50.00% for YAP1. Continuity-corrected McNemar test revealed significant differences in the positive rates of both CDX2 (Table 2, $\chi^2 = 49.020$, $p < 0.001$) and YAP1 (Table 3, $\chi^2 = 38.025$, $p < 0.001$) between GC and paired adjacent noncancerous tissues. Moreover, GC tissues showed significantly higher expression levels than paired adjacent normal tissues (**Supplementary Fig. 1**, $p < 0.001$). These findings indicate that CDX2 and YAP1 exhibit broader positivity and higher expression in GC tissues. As shown in Table 4, no significant differences were observed between the CDX2 low-expression group (N = 40) and CDX2 high-expression group (N = 40) in terms of age, gender, BMI, smoking history, alcohol consumption, diabetes, hypertension, coronary heart disease, family history of cancer, or history of gastrointestinal diseases (Table 4, $p > 0.05$). In addition, no significant differences were found in primary tumor location, tumor diameter, histological differentiation, clinical stage, lymph node metastasis, Hp infection, Lauren classification, PLR, extent of surgical resection, operation time, or pathological type (Table 4, $p > 0.05$). However, compared with the CDX2 low-expression group, the CDX2 high-expression group exhibited lower hemoglobin levels and higher CRP and CEA levels (Table 4, $p < 0.001$). As shown in Table 5, no significant differences were observed between the YAP1 low-expression group (N = 40) and the YAP1 high-expression group (N = 40) in terms of age, BMI, smoking history, alcohol consumption, diabetes, hypertension, coronary heart disease, family history of cancer, history of gastrointestinal diseases, primary tumor location, primary tumor diameter, histological differentiation, clinical stage, lymph node metastasis, Hp infection, Lauren classification, PLR, surgical resection extent, operation time, or pathological classification (Table 5, $p > 0.05$). However, gender distribution differed significantly between the two groups (Table 5, $p = 0.036$), with a higher proportion of males in the YAP1 high-expression group. Furthermore, patients in the YAP1 high-expression group had significantly lower hemoglobin levels ($p = 0.014$), and higher CRP ($p = 0.002$) and CEA levels ($p = 0.015$), compared with those in the YAP1 low-expression group (Table 5). Survival analysis based on CDX2 and YAP1 expression levels revealed no statistically significant differences in overall survival between high- and low-expression subgroups (**Supplementary Fig. 2**, CDX2: Log-rank $\chi^2 = 2.227$, df = 1, $p = 0.1356$; **Supplementary Fig. 3**, YAP1: Log-rank $\chi^2 = 2.735$, df = 1, $p = 0.0982$). The median DFS could not be estimated because the 50% event threshold was not reached in any subgroup during follow-up. Consistently, no significant differences in event risk were observed for CDX2 (HR = 0.423, 95% CI: 0.143–1.255) or YAP1 (HR = 0.395, 95% CI: 0.131–1.188), although the point estimates indicated numerically lower event risks in the low-expression groups compared with the high-expression groups. Spearman correlation analysis showed a weak positive correlation between CDX2 and YAP1 expression; however, this association did not reach statistical significance (Rs = 0.113, $p = 0.319$) (**Supplementary Fig. 4**).

CDX2 Transcriptionally Regulates YAP1 Expression

The expression levels of CDX2 and YAP1 were significantly higher in HGC-27, KATO III, and NCI-N87 cells than in GES-1 cells (Fig. 1A,B, $p < 0.001$). HGC-27 cells, which exhibited the highest expression levels, were

Table 5. Correlation between YAP1 high/low expression and clinical pathological characteristics.

Variable		YAP1 low-expression (N 40)	YAP1 high-expression (N = 40)	$Z/\chi^2/t$	p
Age[n (%)]	≤44	0 (0.00)	0 (0.00)	0.082	0.775
	45-59	8 (20.00)	7 (17.50)		
	≥60	32 (80.00)	33 (82.50)		
Gender [n (%)]	Male	21 (52.50)	30 (75.00)	4.381	0.036
	Female	19 (47.50)	10 (25.00)		
BMI (kg/m^2)		22.45 ± 2.46	22.05 ± 2.17	0.768	0.445
Smoking history [n (%)]		16 (40.00)	14 (35.00)	0.213	0.644
Alcohol consumption [n (%)]		16 (40.00)	20 (50.00)	0.808	0.369
Diabetes [n (%)]		16 (40.00)	22 (55.00)	1.805	0.179
Hypertension [n (%)]		21 (52.50)	22 (55.00)	0.050	0.823
Coronary heart disease [n (%)]		21 (52.50)	26 (65.00)	1.289	0.256
Family history of cancer [n (%)]		5 (12.50)	3 (7.50)	0.139	0.709
History of gastrointestinal diseases [n (%)]	Gastric ulcer	2 (5.00)	2 (5.00)		0.673
	Gastritis	6 (15.00)	9 (22.50)		
	Gastroenteritis	1 (2.50)	3 (7.50)		
	Colon cancer	1 (2.50)	1 (2.50)		
	None	23 (57.50)	22 (55.00)		
	Others	7 (17.50)	3 (7.50)		
Primary tumor location [n (%)]	Upper stomach	11 (27.50)	19 (47.50)	7.137	0.129
	Middle stomach	9 (22.50)	7 (17.50)		
	Lower stomach	15 (37.50)	6 (15.00)		
	Overlapping sites	1 (2.50)	2 (5.00)		
	Unspecified	4 (10.00)	6 (15.00)		
Primary tumor diameter [n (%)]	≤2 cm	12 (30.00)	12 (30.00)	0.000	1.000
	>2 cm	28 (70.00)	28 (70.00)		
Histological differentiation [n (%)]	Well-differentiated	2 (5.00)	6 (15.00)		0.374
	Moderately differentiated	17 (42.50)	14 (35.00)		
	Poorly differentiated	21 (52.50)	20 (50.00)		
	Undifferentiated	0 (0.00)	0 (0.00)		
Clinical stage [n (%)]	1	16 (40.00)	14 (35.00)	0.239	0.811
	2	9 (22.50)	8 (20.00)		
	3	10 (25.00)	17 (42.50)		
	4	5 (12.50)	1 (2.50)		
Lymph node metastasis [n (%)]		19 (47.50)	23 (57.50)	0.802	0.370
Hp infection [n (%)]		29 (72.50)	29 (72.50)	0.000	1.000
Lauren classification [n (%)]	Intestinal type	8 (20.00)	7 (17.50)		0.226
	Diffuse type	20 (50.00)	13 (32.50)		
	Mixed type	12 (30.00)	19 (47.50)		
	Unclassified	0 (0.00)	1 (2.50)		
Hemoglobin (g/L)		80.40 ± 7.61	76.52 ± 6.16	2.509	0.014
CRP (mg/L)		12.13 ± 1.26	12.92 ± 0.99	3.127	0.002
PLR		350.28 ± 53.81	334.02 ± 50.43	1.394	0.167
CEA (μg/L)		6.11 ± 1.08	6.63 ± 0.81	2.478	0.015
Surgical resection extent [n (%)]	Total gastrectomy	12 (30.00)	13 (32.50)	0.058	0.809
	Partial gastrectomy	28 (70.00)	27 (67.50)		
Operation time (h)		4.24 ± 1.13	4.38 ± 0.82	0.634	0.528

Table 5. Continued.

Variable		YAP1 low-expression (N 40)	YAP1 high-expression (N = 40)	$Z/\chi^2/t$	p
Pathological type [n (%)]	Adenocarcinoma	34 (85.00)	33 (82.50)		0.316
	Signet-ring cell carcinoma	3 (7.50)	6 (15.00)		
	Small cell neuroendocrine carcinoma	0 (0.00)	1 (2.50)		
	Poorly cohesive carcinoma	2 (5.00)	0 (0.00)		
	Tubular adenocarcinoma	1 (2.50)	0 (0.00)		

Abbreviation: BMI, body mass index; CRP, C-reactive protein; PLR, platelet-to-lymphocyte ratio; CEA, carcinoembryonic antigen; Hp, *Helicobacter pylori*; YAP1, yes1 associated transcriptional regulator.

selected for the dual-luciferase reporter assay and ChIP assay, while both HGC-27 and KATO III cell lines were used for subsequent functional and molecular experiments. The JASPAR database was used to predict CDX2 binding sites within the YAP1 promoter region (Fig. 1C). To investigate whether CDX2 regulates YAP1 transcription, CDX2 overexpression and shCDX2 constructs were generated. Significant changes in CDX2 levels following transfection were confirmed by qRT-PCR and Western blot analyses, indicating efficient transfection (Fig. 1D–F, $p < 0.05$). The dual-luciferase reporter assay demonstrated that CDX2 significantly enhanced YAP1 promoter transcriptional activity (Fig. 1G, $p < 0.001$). Moreover, ChIP assay results confirmed that CDX2 specifically binds to the YAP1 promoter region (Fig. 1H, $p < 0.001$).

CDX2 Promotes GC Cell Proliferation, Viability and Migration by Inhibiting Ferroptosis via YAP1

YAP1 overexpression and shYAP1 constructs were generated to further investigate the role of YAP1 in GC. Western blot and qRT-PCR analyses confirmed effective modulation of YAP1 expression in HGC-27 cells (**Supplementary Fig. 5A–C**, $p < 0.001$). Similarly, qRT-PCR results verified efficient CDX2 knockdown, as well as YAP1 overexpression and knockdown, in KATO III cells (**Supplementary Fig. 5D,E**, $p < 0.001$). Functional assays showed that CDX2 knockdown significantly suppressed GC cell viability and migration, while YAP1 overexpression partially reversed these inhibitory effects in both HGC-27 and KATO III cells (Fig. 2A–H, $p < 0.05$). Conversely, YAP1 overexpression enhanced cell viability, proliferation, and migration, whereas CDX2 knockdown partially attenuated these effects (Fig. 2A–H, $p < 0.05$). Regarding ferroptosis-related markers, CDX2 knockdown markedly reduced the expression of solute carrier family 7 member 11 (SLC7A11) and GPX4, while increasing Fe^{2+} levels and lipid peroxidation in both cell lines (Fig. 3A–H, Fig. 4A–D, $p < 0.01$). YAP1 overexpression partially reversed these changes (Fig. 3A–H, Fig. 4A–D, $p < 0.05$). Consistently, YAP1 overexpression decreased Fe^{2+} levels and lipid peroxidation, while increasing GPX4 and SLC7A11 expression. Notably, CDX2 knockdown partially abolished the protective effects induced by YAP1 overexpression (Fig. 3A–H, Fig. 4A–D, $p < 0.01$).

Ferrostatin-1 (Fer-1) Rescues YAP1 Knockdown-Mediated Suppression of Malignant Phenotype and Ferroptosis in GC Cells

To further confirm that ferroptosis is the key downstream mechanism mediated by the CDX2/YAP1 axis in GC cells, rescue experiments were performed using the classical ferroptosis inhibitor Fer-1. The results showed that YAP1 knockdown significantly suppressed GC cell viability, proliferation and migration, while these effects were partially reversed by Fer-1 treatment (Fig. 5A–H, $p < 0.05$). Meanwhile, YAP1 knockdown decreased the expression levels of GPX4 and SLC7A11, and increased intracellular Fe^{2+} levels and lipid peroxidation in both HGC-27 and KATO III cells (Fig. 6A–H, Fig. 7A–D, $p < 0.05$). Importantly, Fer-1 treatment partially restored these parameters (Fig. 6A–H, Fig. 7A–D, $p < 0.05$).

Discussion

In this study, we found that CDX2 and YAP1 are highly expressed in GC tissues. Clinically, high expression of CDX2 and YAP1 was associated with lower hemoglobin levels, elevated CRP and CEA levels, and a nonsignificant trend toward poorer overall survival. Mechanistically, our findings demonstrated that CDX2 acts as an upstream transcriptional regulator of YAP1 by directly binding to its promoter region and activating its transcription. Functional assays further confirmed that CDX2 promotes GC cell proliferation and migration through transcriptional activation of YAP1. Collectively, these findings identify the CDX2/YAP1 axis as a key molecular pathway contributing to GC malignant progression and provide new insights into the regulatory mechanisms underlying GC development.

Ferroptosis is an iron-dependent, lipid-peroxidation-driven form of regulated cell death that differs mechanistically from necrosis, autophagy, and apoptosis [21,22,23]. During this process, excessive Fe^{2+} promotes the initiation and propagation of lipid peroxidation, thereby triggering ferroptosis [24]. GPX4 and SLC7A11 are key components of the ferroptosis defense system: GPX4 prevents ferrop-

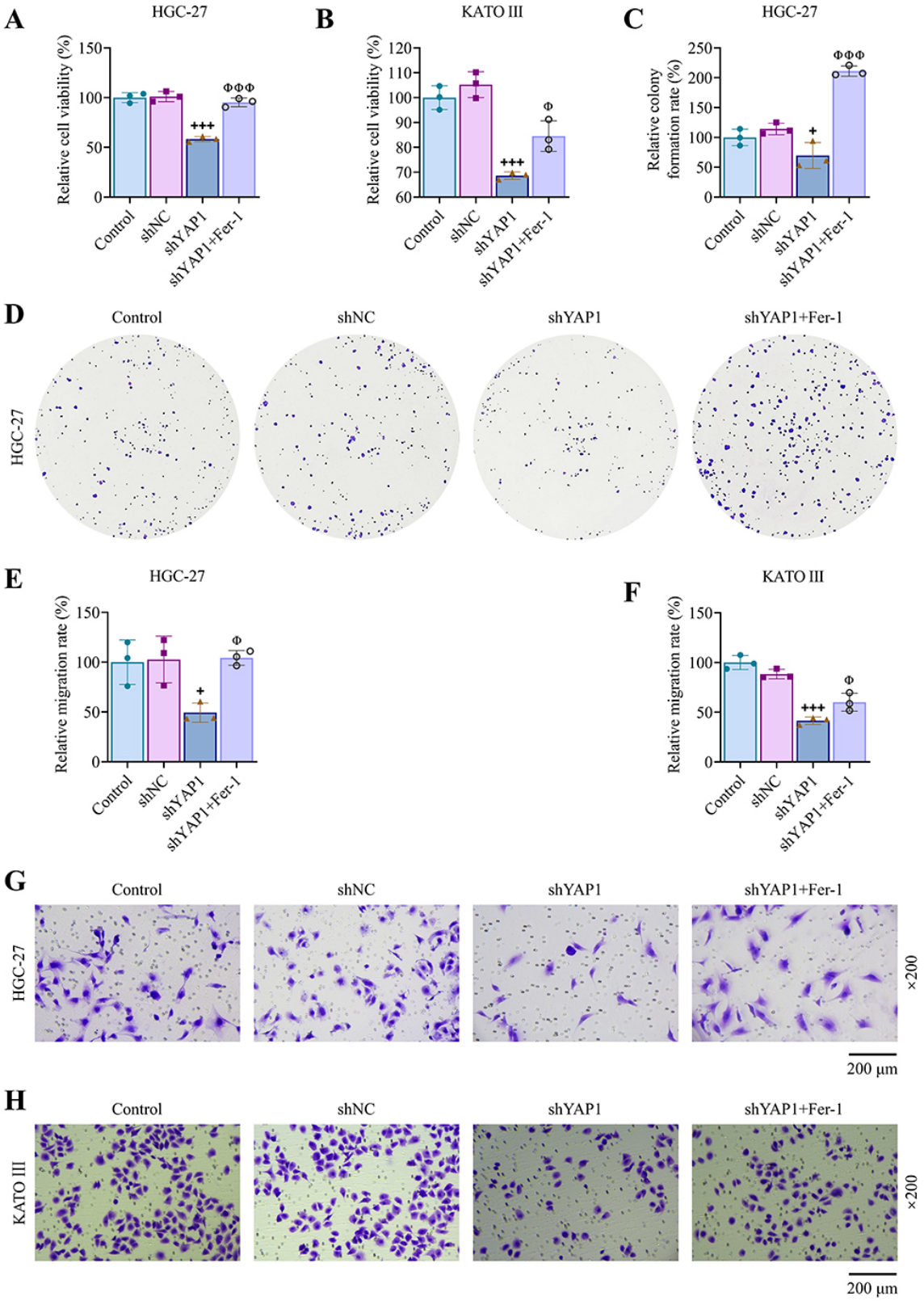

Fig. 5. Effects of YAP1 and ferrostatin-1 (Fer-1) on cell function. (A,B) CCK-8 assays assessing the viability of HGC-27 cells and KATO III cells in the following groups: Control, shNC, shYAP1, and shYAP1+Fer-1. (C,D) Colony formation assays assessing the proliferative capacity of HGC-27 cells. (E–H) Transwell assays evaluating cell migration of HGC-27 or KATO III cells. Magnification: 200×; scale bar: 200 μm. All experiments were independently repeated three times with three biological replicates. $^{+}p < 0.05$, $^{+++}p < 0.001$ vs. shNC; $^{\Phi}p < 0.05$, $^{\Phi\Phi\Phi}p < 0.001$ vs. shYAP1 (one-way ANOVA followed by Tukey's multiple comparisons test).

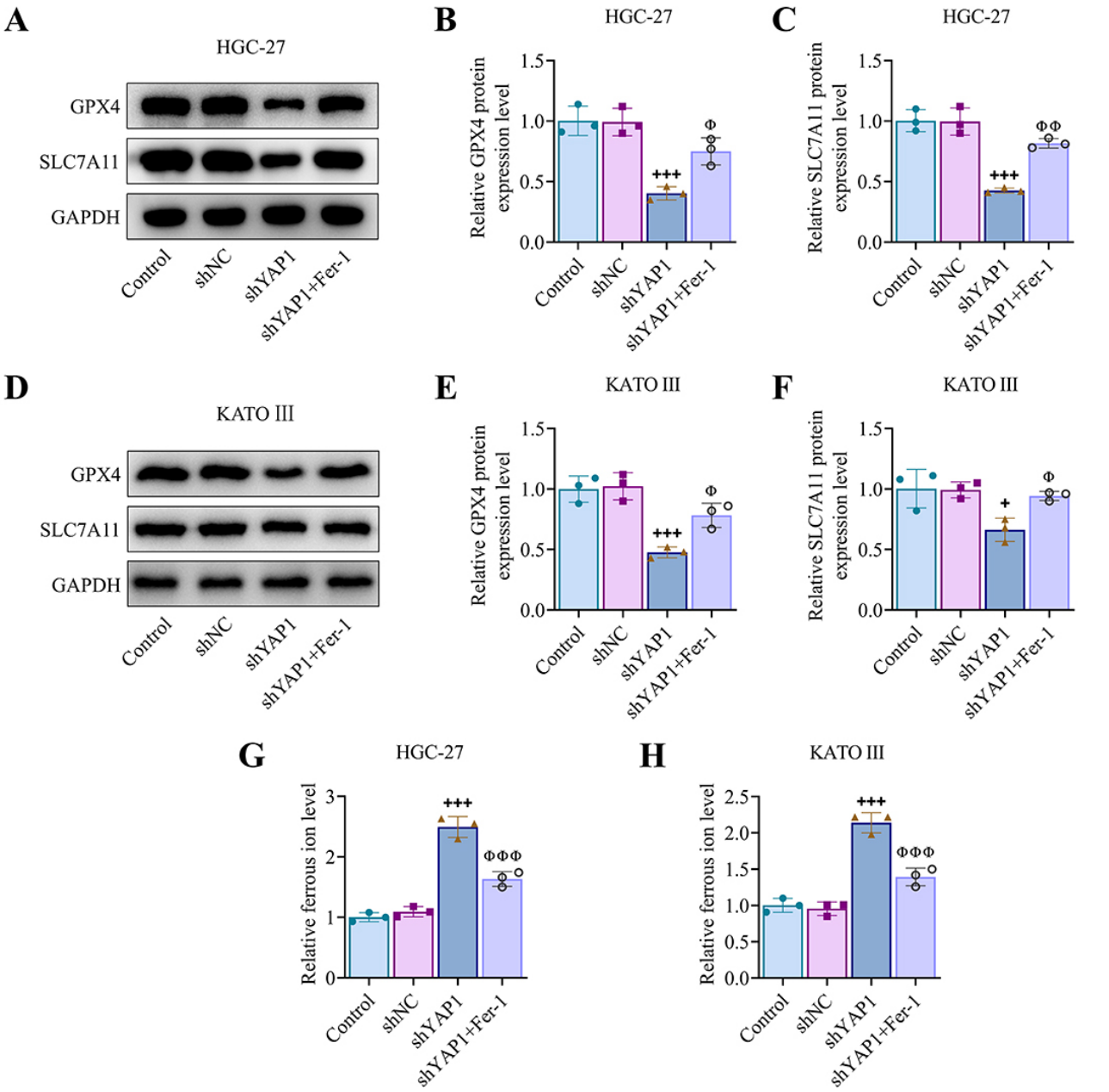

Fig. 6. Fer-1 partially reverses YAP1 knockdown-induced ferroptosis. (A–F) Western blot analysis of GPX4 and SLC7A11 protein levels in HGC-27 or KATO III cells. GAPDH was used as an internal control. (G,H) Detection of ferrous ion levels in HGC-27 and KATO III cells using a commercial kit across the indicated groups, with all data normalized to the Control group. All experiments were independently repeated three times with three biological replicates. $^{+}p < 0.05$, $^{+++}p < 0.001$ vs. shNC; $^{\Phi}p < 0.05$, $^{\Phi\Phi}p < 0.01$, $^{\Phi\Phi\Phi}p < 0.001$ vs. shYAP1 (one-way ANOVA followed by Tukey's multiple comparisons test).

tosis by detoxifying lipid peroxides and protecting membrane integrity [25], while SLC7A11 promotes cystine uptake to facilitate glutathione (GSH) synthesis, thereby indirectly supporting GPX4 activity [26]. Accumulating evidence suggests that ferroptosis evasion contributes to malignant progression and therapeutic resistance in GC. For instance, cystatin SN (CST1) suppresses ferroptosis and promotes metastasis by stabilizing GPX4 protein through the deubiquitinase ovarian tumor domain-containing protein 1 (OTUB1) in GC [27]. Similarly, actin-like protein 6A (ACTL6A) protects GC cells from ferroptosis by enhancing GSH synthesis [28]. In addition, tumor-associated fibroblast (CAF)-derived exosomal miR-522 inhibits ferroptosis, contributing to acquired chemoresistance in GC [29]. These studies underscore the critical role of ferroptosis evasion in GC cell survival and progression. In our study, YAP1 knockdown significantly reduced GPX4 and SLC7A11 expression, accompanied by increased Fe^{2+} ac-

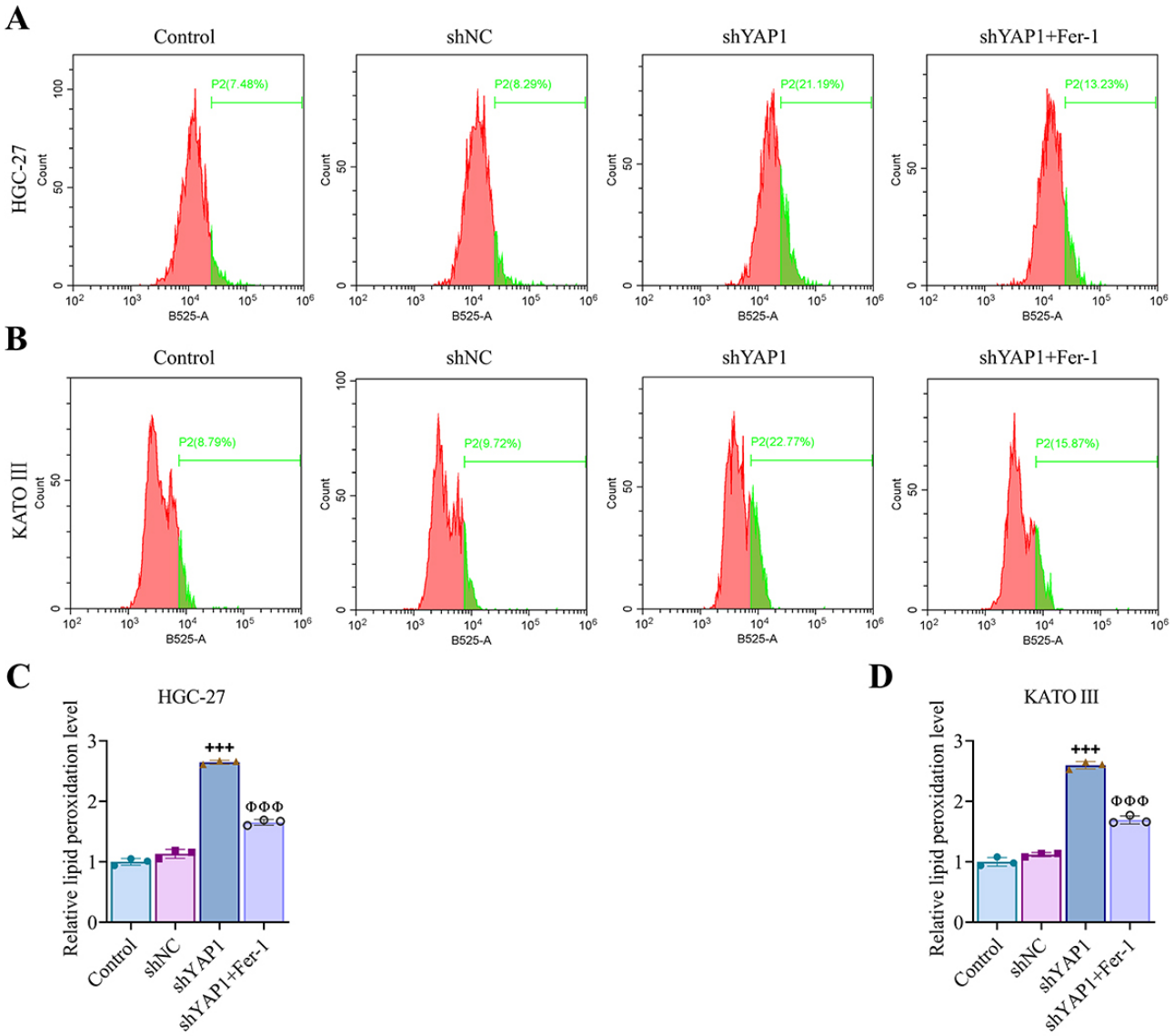

Fig. 7. Fer-1 partially reverses YAP1 knockdown-induced lipid peroxidation levels. (A–D) Detection of lipid peroxidation levels in HGC-27 and KATO III cells using C11-BODIPY 581/591 fluorescent probe, with all data normalized to the Control group. All experiments were independently repeated three times with three biological replicates. $^{+++}p < 0.001$ vs. shNC; $^{\Phi\Phi\Phi}p < 0.001$ vs. shYAP1 (one-way ANOVA followed by Tukey's multiple comparisons test).

cumulation and lipid peroxidation, indicating the induction of ferroptosis. Notably, treatment with the ferroptosis inhibitor Fer-1 partially reversed these effects and alleviated ferroptotic responses. These findings are consistent with previous studies demonstrating that YAP1 promotes ferroptosis resistance in contexts such as sepsis-induced organ injury and hepatoblastoma [30,31,32]. Collectively, these results support the pivotal role of YAP1 in regulating ferroptosis.

Nevertheless, the upstream regulatory mechanisms underlying YAP1-mediated ferroptosis suppression in GC remain poorly understood. In this study, we further demonstrated that CDX2 transcriptionally activates YAP1, thereby inhibiting ferroptosis and promoting malignant progression in GC. Notably, the biological role of CDX2 in GC remains controversial. A previous study has identified CDX2 as a classic tumor suppressor, with its overexpression associated with improved prognosis in GC [33]. Consistently, exogenous overexpression of CDX2 has been shown to suppress cell proliferation and epithelial-mesenchymal transition (EMT) in specific GC cell lines, such as MKN45 [34]. However, accumulating clinical evidence also suggests a potential oncogenic role of CDX2 in GC. Song et al. [12] reported that CDX2 is rarely expressed in normal gastric epithelium but is frequently induced during gastric carcinogenesis, particularly during the development of intestinal-type GC. A clinical cohort study has further shown that CDX2 positivity is significantly increased in GC tissues

compared with matched normal mucosa and is closely associated with lymph node metastasis [35]. However, this association was not observed in our cohort, which may be attributable to differences in patient populations, sample sizes, and criteria for evaluating CDX2 expression. In addition, a functional study in colorectal cancer has further demonstrated that CDX2 overexpression promotes malignant cell proliferation, suggesting that CDX2 positivity may confer pro-tumorigenic properties [36]. Consistent with these findings, our study revealed that CDX2 transcriptionally upregulates YAP1, thereby suppressing ferroptosis. This regulatory pathway ultimately promotes GC cell proliferation, migration, and viability. Moreover, we observed widespread expression of both CDX2 and YAP1 in GC tissues. High CDX2 and YAP1 expression was associated with lower hemoglobin levels, elevated CRP and CEA levels, and unfavorable overall survival in GC patients. These clinical observations, together with our *in vitro* mechanistic findings, collectively suggest that the CDX2/YAP1 axis may play an important role in GC malignant progression.

Notwithstanding the new insights provided by this study, several limitations should be acknowledged. First, the study cohort included only 80 paired GC and adjacent normal tissue samples from a single center, which may limit the generalizability of our findings. In addition, median split dichotomization based on continuous MOD values from IHC staining was performed solely to balance the sample sizes of the high- and low-expression subgroups. This artificial binary classification inevitably results in the loss of quantitative information regarding staining intensity and may introduce potential statistical bias. Second, all functional validations of the CDX2/YAP1/ferroptosis regulatory axis were conducted in cell-based experiments and lacked comprehensive *in vivo* validation using animal models. Although we assessed key ferroptosis-related parameters, including iron accumulation, lipid peroxidation levels, and the expression of canonical ferroptosis regulators, we did not establish ferroptosis-resistant cell models. Furthermore, classic ferroptosis inducers (e.g., erastin and RSL3) were not applied to further evaluate cellular sensitivity and resistance to ferroptosis. Given the complexity of the tumor microenvironment, cell-cell interactions, and systemic metabolic conditions in human tumors, further studies using xenograft or genetically engineered mouse models are warranted to validate the role of the CDX2/YAP1/ferroptosis axis in GC progression under physiological conditions.

Conclusion

In conclusion, our study demonstrates that CDX2 promotes gastric cancer progression by transcriptionally activating YAP1, which subsequently suppresses ferroptosis through upregulation of GPX4 and SLC7A11 and reduction of Fe^{2+} accumulation and lipid peroxidation. Clinically, both CDX2 and YAP1 are widely expressed in GC tissues, and their high expression is associated with lower hemoglobin levels, elevated CRP and CEA levels, and a nonsignificant trend toward poorer overall survival. These findings expand the current understanding of ferroptosis regulation in GC and suggest that the CDX2/YAP1 axis may represent a potential target for future therapeutic exploration. Targeting this pathway may enhance GC cell sensitivity to ferroptosis-inducing therapies, providing a mechanistic foundation for subsequent anti-tumor research.

Availability of Data and Materials

The analyzed datasets generated during the study are available from the corresponding author on reasonable request.

Author Contributions

DQZ and HJR designed the research study; LHY and MLG performed the research; JJF and SJZ collected and analyzed the data. SJZ has been involved in drafting the manuscript and all authors have been involved in revising it critically for important intellectual content. All authors gave final approval of the version to be published. All authors have participated sufficiently in the work to take public responsibility for appropriate portions of the content and agreed to be accountable for all aspects of the work in ensuring that questions related to its accuracy or integrity are appropriately investigated and resolved.

Ethics Approval and Consent to Participate

This study was approved by The First People's Hospital of Lin'an District Ethics Committee (Approval No. Lin'an First People's Hospital Lun Yan Shen No. 21 of 2023). Written informed consent was obtained from all participants enrolled in this study. All experimental procedures involving human participants were performed in accordance with the principles outlined in the Declaration of Helsinki.

Acknowledgment

Not applicable.

Funding

This work was supported by Research Guidance Project for Agricultural and Social Development of Lin'an District, Hangzhou City (grant number: 2022Y15).

Conflict of Interest

The authors declare no conflict of interest.

Supplementary Material

Supplementary material associated with this article can be found, in the online version, at https://doi.org/10.24976/Discov.Med.202638214.271.

References

[1] Shin WS, Xie F, Chen B, Yu P, Yu J, To KF, et al. Updated Epidemiology of Gastric Cancer in Asia: Decreased Incidence but Still a Big Challenge. Cancers. 2023; 15: 2639. https://doi.org/10.3390/cancers15092639

[2] Li Y, Hahn AI, Laszkowska M, Jiang F, Zauber AG, Leung WK. Global burden of young-onset gastric cancer: a systematic trend analysis of the global burden of disease study 2019. Gastric Cancer: Official Journal of the International Gastric Cancer Association and the Japanese Gastric Cancer Association. 2024; 27: 684–700. https://doi.org/10.1007/s10120-024-01494-6

[3] Dincă AL, Meliț LE, Mărginean CO. Old and New Aspects of H. pylori-Associated Inflammation and Gastric Cancer. Children (Basel, Switzerland). 2022; 9: 1083. https://doi.org/10.3390/children9071083

[4] Kang K, Bagaoisan MA, Zhang Y. Unveiling the Younger Face of Gastric Cancer: A Comprehensive Review of Epidemiology, Risk Factors, and Prevention Strategies. Cureus. 2024; 16: e62826. https://doi.org/10.7759/cureus.62826

[5] Koustas E, Trifylli EM, Sarantis P, Papadopoulos N, Karapedi E, Aloizos G, et al. Immunotherapy as a Therapeutic Strategy for Gastrointestinal Cancer-Current Treatment Options and Future Perspectives. International Journal of Molecular Sciences. 2022; 23: 6664. https://doi.org/10.3390/ijms23126664

[6] Li Y, Feng A, Zheng S, Chen C, Lyu J. Recent Estimates and Predictions of 5-Year Survival in Patients with Gastric Cancer: A Model-Based Period Analysis. Cancer Control: Journal of the Moffitt Cancer Center. 2022; 29: 10732748221099227. https://doi.org/10.1177/10732748221099227

[7] Hu X, Zhang Y, Yu H, Zhao Y, Sun X, Li Q, et al. The role of YAP1 in survival prediction, immune modulation, and drug response: A pan-cancer perspective. Frontiers in Immunology. 2022; 13: 1012173. https://doi.org/10.3389/fimmu.2022.1012173

[8] Qiu D, Gao L, Yu X. Knockdown of YAP1 Reduces YTHDF3 to Stabilize SMAD7 and thus Inhibit Bladder Cancer Stem Cell Stemness. Discovery Medicine. 2024; 36: 1486–1498. https://doi.org/10.24976/Discov.Med.202436186.138

[9] Wu J, Minikes AM, Gao M, Bian H, Li Y, Stockwell BR, et al. Intercellular interaction dictates cancer cell ferroptosis via NF2-YAP signalling. Nature. 2019; 572: 402–406. https://doi.org/10.1038/s41586-019-1426-6

[10] Fu X, Wu H, Li C, Deng G, Chen C. YAP1 inhibits RSL3-induced castration-resistant prostate cancer cell ferroptosis by driving glutamine uptake and metabolism to GSH. Molecular and Cellular Biochemistry. 2024; 479: 2415–2427. https://doi.org/10.1007/s11010-023-04847-4

[11] Larsen S, Davidsen J, Dahlgaard K, Pedersen OB, Troelsen JT. HNF4α and CDX2 Regulate Intestinal YAP1 Promoter Activity. International Journal of Molecular Sciences. 2019; 20: 2981. https://doi.org/10.3390/ijms20122981

[12] Song X, Chen H, Shen B, Bai A, Wang J, Li X, et al. Expression of Cdx2 and claudin-2 in the multistage tissue of gastric carcinogenesis. Oncology. 2007; 73: 357–365. https://doi.org/10.1159/000135351

[13] Jahan S, Awaja N, Hess B, Hajjar S, Sad S, Lohnes D. The transcription factor Cdx2 regulates inflammasome activity through expression of the NLRP3 suppressor TRIM31 to maintain intestinal homeostasis. The Journal of Biological Chemistry. 2022; 298: 102386. https://doi.org/10.1016/j.jbc.2022.102386

[14] Yu J, Li S, Xu Z, Guo J, Li X, Wu Y, et al. CDX2 inhibits epithelial-mesenchymal transition in colorectal cancer by modulation of Snail expression and β-catenin stabilisation via transactivation of PTEN expression. British Journal of Cancer. 2021; 124: 270–280. https://doi.org/10.1038/s41416-020-01148-1

[15] Lopes N, Bergsland C, Bruun J, Bjørnslett M, Vieira AF, Mesquita P, et al. A panel of intestinal differentiation markers (CDX2, GPA33, and LI-cadherin) identifies gastric cancer patients with favourable prognosis. Gastric Cancer: Official Journal of the International Gastric Cancer Association and the Japanese Gastric Cancer Association. 2020; 23: 811–823. https://doi.org/10.1007/s10120-020-01064-6

[16] Wang Q, Zhang C, Cao S, Zhao H, Jiang R, Li Y. Tumor-derived exosomes orchestrate the microRNA-128-3p/ELF4/CDX2 axis to facilitate the growth and metastasis of gastric cancer via delivery of LINC01091. Cell Biology and Toxicology. 2023; 39: 519–536. https://doi.org/10.1007/s10565-022-09728-y

[17] Wang FH, Zhang XT, Li YF, Tang L, Qu XJ, Ying JE, et al. The Chinese Society of Clinical Oncology (CSCO): Clinical guidelines for the diagnosis and treatment of gastric cancer, 2021. Cancer Communications (London, England). 2021; 41: 747–795. https://doi.org/10.1002/cac2.12193

[18] Lu H, Yao J, Xue C, Huang R, Huang B. Immune analysis according to Lauren type for gastric cancer and its significance in individual treatment and prognostic prediction. Frontiers in Immunology. 2025; 16: 1589513. https://doi.org/10.3389/fimmu.2025.1589513

[19] Guerrero-Hue M, García-Caballero C, Palomino-Antolín A, Rubio-Navarro A, Vázquez-Carballo C, Herencia C, et al. Curcumin reduces renal damage associated with rhabdomyolysis by decreasing ferroptosis-mediated cell death. FASEB Journal: Official Publication of the Federation of American Societies for Experimental Biology. 2019; 33: 8961–8975. https://doi.org/10.1096/fj.201900077R

[20] Damgaard MV, Treebak JT. Protocol for qPCR analysis that corrects for cDNA amplification efficiency. STAR Protocols. 2022; 3: 101515. https://doi.org/10.1016/j.xpro.2022.101515

[21] Wang B, Wang Y, Zhang J, Hu C, Jiang J, Li Y, et al. ROS-induced lipid peroxidation modulates cell death outcome: mechanisms behind apoptosis, autophagy, and ferroptosis. Archives of Toxicology. 2023; 97: 1439–1451. https://doi.org/10.1007/s00204-023-03476-6

[22] Ai Y, Meng Y, Yan B, Zhou Q, Wang X. The biochemical pathways of apoptotic, necroptotic, pyroptotic, and ferroptotic cell death. Molecular Cell. 2024; 84: 170–179. https://doi.org/10.1016/j.molcel.2023.11.040

[23] Wang G, Li S, Li F, Zhang Z. Bone Marrow Mesenchymal Stem Cells Inhibit Ferroptosis Through Mitochondrial Transfer and Improve Endothelial Cell Dysfunction. Discovery Medicine. 2025; 37: 1372–1384. https://doi.org/10.24976/Discov.Med.202537198.119

[24] Cao J, Chen X, Chen L, Lu Y, Wu Y, Deng A, et al. DHODH-mediated mitochondrial redox homeostasis: a novel ferroptosis regulator and promising therapeutic target. Redox Biology. 2025; 85: 103788. https://doi.org/10.1016/j.redox.2025.103788

[25] Ma T, Du J, Zhang Y, Wang Y, Wang B, Zhang T. GPX4-independent ferroptosis-a new strategy in disease's therapy. Cell Death Discovery. 2022; 8: 434. https://doi.org/10.1038/s41420-022-01212-0

[26] Jyotsana N, Ta KT, DelGiorno KE. The Role of Cystine/Glutamate Antiporter SLC7A11/xCT in the Pathophysiology of Cancer. Frontiers in Oncology. 2022; 12: 858462. https://doi.org/10.3389/fonc.2022.858462

[27] Li D, Wang Y, Dong C, Chen T, Dong A, Ren J, et al. CST1 inhibits ferroptosis and promotes gastric cancer metastasis by

regulating GPX4 protein stability via OTUB1. Oncogene. 2023; 42: 83–98. https://doi.org/10.1038/s41388-022-02537-x

[28] Yang Z, Zou S, Zhang Y, Zhang J, Zhang P, Xiao L, et al. ACTL6A protects gastric cancer cells against ferroptosis through induction of glutathione synthesis. Nature Communications. 2023; 14: 4193. https://doi.org/10.1038/s41467-023-39901-8

[29] Zhang H, Deng T, Liu R, Ning T, Yang H, Liu D, et al. CAF secreted miR-522 suppresses ferroptosis and promotes acquired chemo-resistance in gastric cancer. Molecular Cancer. 2020; 19: 43. https://doi.org/10.1186/s12943-020-01168-8

[30] Wang J, Zhu Q, Li R, Zhang J, Ye X, Li X. YAP1 protects against septic liver injury via ferroptosis resistance. Cell & Bioscience. 2022; 12: 163. https://doi.org/10.1186/s13578-022-00902-7

[31] Yang X, Duan H, Li S, Zhang J, Dong L, Ding J, et al. Yap1 alleviates sepsis associated encephalopathy by inhibiting hippocampus ferroptosis via maintaining mitochondrial dynamic homeostasis. Journal of Cellular and Molecular Medicine. 2024; 28: e70156. https://doi.org/10.1111/jcmm.70156

[32] Zhu G, Xie Y, Bian Z, Ma J, Zhen N, Chen T, et al. N6-methyladenosine modification of LATS2 promotes hepatoblastoma progression by inhibiting ferroptosis through the YAP1/ATF4/PSAT1 axis. International Journal of Biological Sciences. 2024; 20: 4146–4161. https://doi.org/10.7150/ijbs.92413

[33] Khayyat A, Esmaeil Pour MA, Poursina O, Zohouri SA, Jian PV, Patel N, et al. Evaluations of Biomarkers CDX1 and CDX2 in Gastric Cancer Prognosis: A Meta-analysis. International Journal of Molecular and Cellular Medicine. 2024; 13: 1–19. https://doi.org/10.22088/IJMCM.BUMS.13.1.1

[34] Zhang JF, Qu LS, Qian XF, Xia BL, Mao ZB, Chen WC. Nuclear transcription factor CDX2 inhibits gastric cancer-cell growth and reverses epithelial-to-mesenchymal transition in vitro and in vivo. Molecular Medicine Reports. 2015; 12: 5231–5238. https://doi.org/10.3892/mmr.2015.4114

[35] Samadani AA, Nikbakhsh N, Taheri H, Shafaee S, Fattahi S, Pilehchian Langroudi M, et al. CDX1/2 and KLF5 Expression and Epigenetic Modulation of Sonic Hedgehog Signaling in Gastric Adenocarcinoma. Pathology Oncology Research: POR. 2019; 25: 1215–1222. https://doi.org/10.1007/s12253-019-00594-4

[36] Salari K, Spulak ME, Cuff J, Forster AD, Giacomini CP, Huang S, et al. CDX2 is an amplified lineage-survival oncogene in colorectal cancer. Proceedings of the National Academy of Sciences of the United States of America. 2012; 109: E3196–E3205. https://doi.org/10.1073/pnas.1206004109